NANO LETTERS

2008
Vol. 8, No. 4
1224-1228

Direct Transmission Detection of Tunable Mechanical Resonance in an Individual Carbon Nanofiber Relay

Anders Eriksson,[†] SangWook Lee,[†,‡] Abdelrahim A. Sourab,[†] Andreas Isacsson,[§] Risto Kaunisto,[||] Jari M. Kinaret,[§] and Eleanor E. B. Campbell*[,†,⊥]

Department of Physics, Göteborg University, Göteborg SE-412 96, Sweden, Department of Physics, Konkuk University, Seoul 143-701, Korea, Department of Applied Physics, Chalmers University of Technology, SE-412 96 Göteborg, Sweden, Nokia Research Center, Nokia Group, P.O. Box 407, FIN-00045 Helsinki, Finland, and School of Chemistry, Edinburgh University, West Mains Road, Edinburgh EH9 3JJ, Scotland

Received February 4, 2008; Revised Manuscript Received February 21, 2008

ABSTRACT

A direct on-chip transmission measurement of the resonance frequency of an individual singly clamped carbon nanofiber relay is reported. The experimental results are in good agreement with a small signal model and show the expected tuning of the resonance frequency with changing bias voltage.

Nanoelectromechanical systems (NEMS) are attracting increasing attention due to their small size, low power consumption, and fast switching speeds.[1] They are regarded as among the most interesting emerging technologies on the ITRS roadmap.[2] Carbon nanotubes are particularly interesting as NEMS components due to their low mobile mass and high Young's modulus, which enables high speed, combined with their high mechanical strength and ability to withstand extreme conditions of temperature and radiation exposure. The predicted possibility of tuning the resonance frequency over a large range by the application of a gate voltage[3] is particularly promising for many applications. Here we present a direct transmission measurement of the resonance frequency of an individual singly clamped carbon nanofiber relay. The experimental results verify the predictions of a small signal model and provide important information for determining the practicality of using carbon-based NEMS as components in real electrical circuits.

Some prototype carbon NEMS have been reported in the literature,[4–11] but there have been relatively few experimental studies of the high frequency properties of carbon NEMS based on individual carbon nanotubes.[12–16] The resonance frequencies of doubly clamped suspended single-walled nanotubes (SWNT) have been determined using an indirect mixing technique with a lock-in amplifier.[12–14] The method requires a semiconducting nanotube and can therefore not be applied to the mechanically more rigid multiwalled nanotubes (MWNT) or nanofibers (CNF) that have been studied as a dc prototype NEMS and allow the fabrication of more varied device geometries.[4–8,10,11] The mechanical resonances of singly clamped MWNT have been observed in a field emission microscope, where the broadening of the field emission spot was observed as the nanotube was brought into mechanical resonance by the application of an ac voltage on a side gate. The resonance frequency of the MWNT could be tuned by an order of magnitude by increasing the bias voltage on the nanotube and thus increasing the tension.[15] The same technique has recently been used to demonstrate a so-called nanoradio.[16] Although all of these studies provide interesting information concerning the resonance properties of individual carbon nanotubes, they do not provide much-needed information on the feasibility of integrating carbon-based NEMS in useful electronic circuits nor on the signal levels that can be expected. In this letter, we report the first direct transmission detection of the resonant behavior of a two-terminal carbon nanofiber relay. We compare the experimental data with the predictions of a small signal model, treating the CNF as a simple series resonator. Good agreement is obtained concerning the resonance amplitude, shape, and phase. We show that it is possible to measure the transmission of a single relay device; however, the signal level is very low and most practical applications will need to be based on arrays of such structures.

A schematic diagram of the device is shown in Figure 1, along with the substrate layout and equivalent circuit model. The small signal model is expected to be valid if the bias voltage applied between the source and the drain electrode,

* Corresponding author. E-mail: Eleanor.Campbell@ed.ac.uk.
[†] Department of Physics, Göteborg University.
[‡] Department of Physics, Konkuk University.
[§] Department of Applied Physics, Chalmers University of Technology.
[||] Nokia Research Center.
[⊥] School of Chemistry, Edinburgh University.

10.1021/nl080345w CCC: $40.75
Published on Web 03/06/2008

V_{SD}, is much greater than the amplitude of the ac voltage applied in series at the source electrode, V_{AC}, i.e., in the regime of linear response. When a dc bias voltage is applied, the CNF becomes charged with respect to the drain electrode and a capacitive coupling is induced. If the CNF is at mechanical resonance, the electric field will vary harmonically, thus inducing a surface current at the drain electrode that can be detected.

The equivalent motional parameters for the resonator, Figure 1b, are given by ref 17:

$$L_m = \frac{m_{eff}}{V_{SD}^2 \cdot C_D'(x)}; \quad C_m = \frac{1}{L_m \cdot \omega^2}; \quad R_m = \frac{\omega_0}{Q_0} L_m + R_C \quad (1)$$

where $m_{eff} \approx m/5.684$ is the effective mass of the CNF (m is its physical mass), V_{SD} is the dc bias voltage, ω_0 and ω are the intrinsic and tuned resonant frequencies of the CNF, Q_0 is the intrinsic mechanical/frictional Q-factor of the resonator, and R_C is the contact resistance between the resonator and the source electrode. The derivative of the capacitance at the quiescent point, $C_D'(x)$, is given by:

$$C_D'(x) = \frac{C_{D0}\Delta_{CNF-drain}}{(\Delta_{CNF-drain} - x)^2} \quad (2)$$

where $\Delta_{CNF-drain}$ is the static unbiased equilibrium distance between the suspended CNF and the drain electrode, x is the static down-deflection of the CNF for a given dc bias, V_{SD}, and C_{D0} is the static unbiased equilibrium capacitance between the CNF and the drain electrode.[18] The motional inductance and capacitance are thus determined theoretically by the geometry of the device, the Young's modulus of the CNF, and the applied bias voltage, V_{SD}. The motional resistance is then set by the intrinsic Q-factor, Q_0, and the contact resistance, R_C

$$\frac{1}{Q_L} = \frac{1}{Q_{R_m}} + \frac{1}{Q_{R_L}} = \frac{\omega_0}{\omega \cdot Q_0} + \frac{R_C}{\omega \cdot L_m} + \frac{Z_{in} + Z_{out}}{\omega \cdot L_m} \quad (3)$$

where Z_{in} and Z_{out} are the input and output impedance, respectively (Figure 1b, $Z_{in} = 50\ \Omega$, $Z_{out} = 100\ \Omega$). The expression is dominated by the first term.

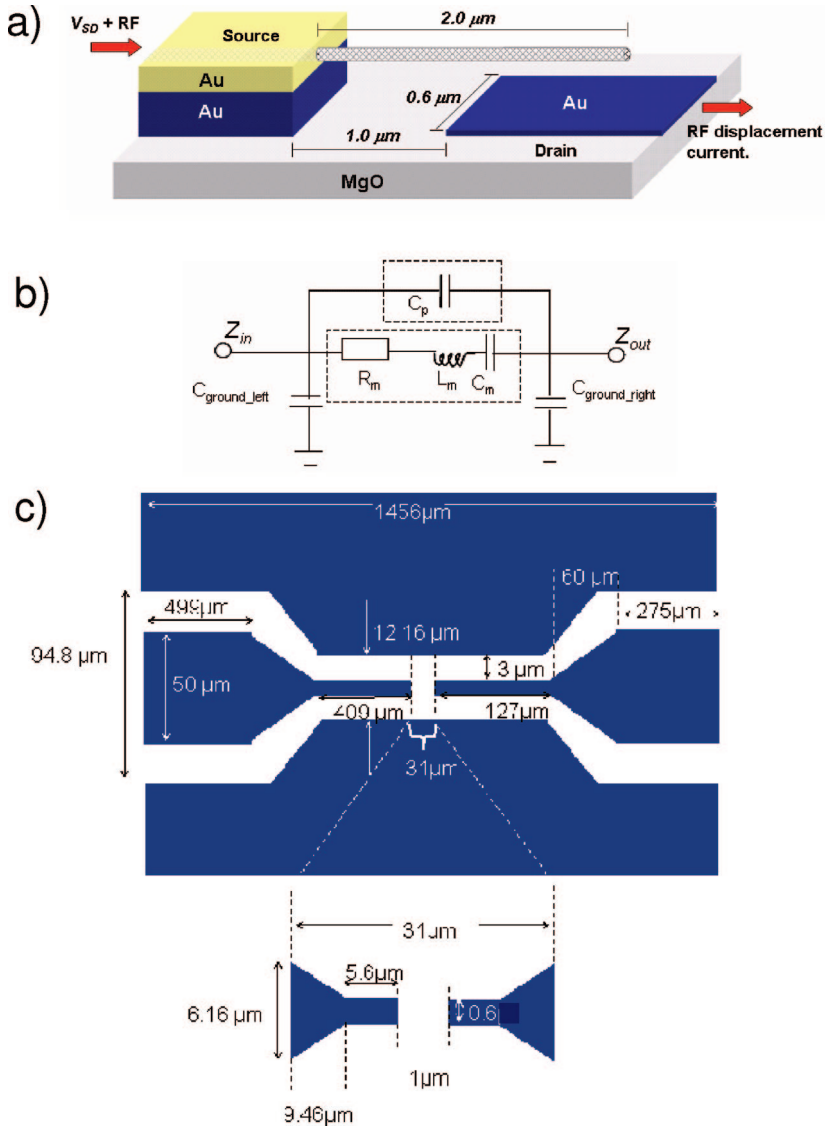

Figure 1. (a) Schematic drawing of two-terminal CNF relay. (b) Equivalent circuit. (c) Substrate layout, designed to reduce parasitic capacitance. Note, drawing is not to scale.

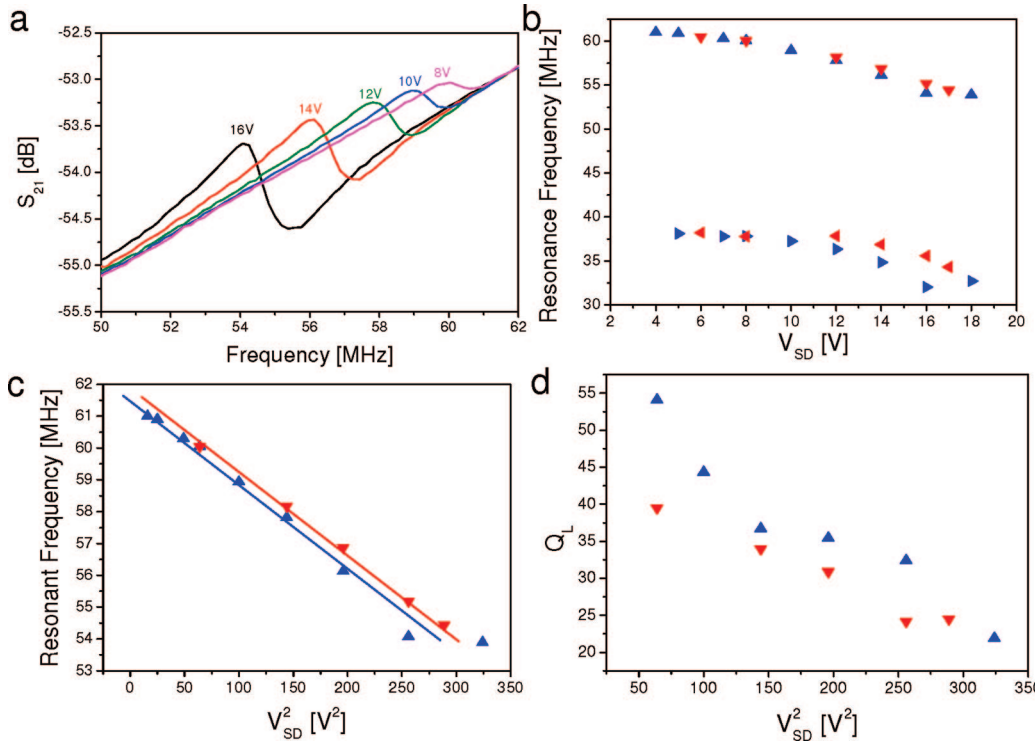

Figure 2. (a) Transmission signal, S_{21} parameter, for a two-terminal CNF relay. The resonance frequency is tuned downward as the source−drain voltage, V_{SD}, is increased. (b) Resonance frequency vs V_{SD} for two resonators. Blue symbols (up- and right-pointing-triangles), forward voltage scan. Red symbols (down- and left-pointing-triangles), reverse voltage scan. (c) Resonant frequency vs V_{SD}^2 for the higher of the two resonances shown in (b). The frequency shift is linear with V_{SD}^2 as expected from the small signal model. The departure from linear behavior at high voltages and the slight shift upward in frequency on the reverse scan is attributed to geometrical changes occurring on the first voltage scan. (d) The loaded Q-factor, Q_L, obtained from the fitted motional impedance parameters for the high frequency resonator.

A magnesium oxide single crystal wafer (Tateho Chemical Industries Co. Ltd.) was chosen as substrate. MgO has a similar dielectric constant (9.65 at 1 MHz) to alumina (9.6 at 1 MHz), which is normally used as a substrate for RF measurements and is also employed in standard SOLT ("short", "open", "load", "through") calibration substrates. The smooth epi-polished surface of the MgO proved to be more suitable for nanoscale electrode fabrication than the commercially available alumina substrates. The micrometer scale coplanar waveguide and ground plate region were patterned by photolithography, whereas the nanometer scale source and drain electrodes were patterned in between the coplanar lines using e-beam lithography. The source electrode was patterned to have its surface lying 220 nm above that of the drain electrode (note, however, that the suspended nanostructure may not be exactly horizontal and the distance of the tip to the drain electrode may be less than the electrode height difference). The relay device is prepared by depositing dispersed carbon nanofibers using ac dielectrophoresis. The method has been described previously[19] and was used to fabricate prototype three-terminal nanorelays.[4] Because of the highly insulating nature of the substrate, it is not possible to image the device using electron microscopy. For this reason, we have had to use relatively large (50–100 nm diameter, 2–3 μm long) carbon nanofibers prepared by dc plasma-enhanced chemical vapor deposition.[20] These structures are just large enough to be imaged with a good optical microscope, which allows us to check for the presence and alignment of the carbon nanostructure before the RF measurements. Although these nanostructures are mainly hollow (typically with bamboo-like partitioning), they do not have the highly crystalline structure of good quality multi-walled nanotubes and we prefer to refer to them as nanofibers to clarify this distinction. Arrays of carbon nanofibers are grown on a Si wafer and then removed and dispersed in sodium dodecyl sulfate (SDS) before being deposited on the source electrode in the presence of a 16 V peak-to-peak ac voltage at a frequency of 13 MHz. After all fabrication steps have been completed, the device is checked in an optical microscope and then mounted on a printed circuit board containing an operational amplifier circuit. *S*-parameter measurements were performed using an Agilent ENA network analyzer (E7501B). Calibration was done using a SOLT CS-5 calibration substrate and "ground"−"signal"−"ground" (GSG) probes with 200 μm pitch were employed for all measurements. All experiments were done under high vacuum conditions (5×10^{-8} Torr) at room temperature. After measurement, the device geometry was checked in a scanning electron microscope after the evaporation of a 25 nm thick gold film to avoid charging problems.

The substrate layout, Figure 1c, has been designed to minimize parasitic cross-talk, making it feasible to realize a broadband detection scheme using transmission detection with a standard network analyzer. A similar approach was followed by Husain et al. for measurements on a platinum nanowire resonator.[21] The simulated (MOMENTUM ADS)

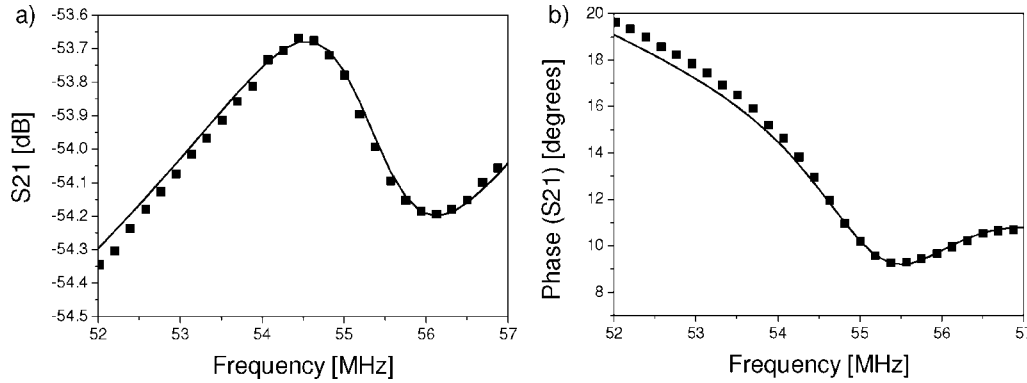

Figure 3. (a) Amplitude S_{21} and (b) phase for the high frequency resonance with $V_{SD} = 17$ V. The experimental data is shown as square symbols. The full lines are obtained from assuming small signal model behavior and simulating the entire system in the ADS circuit simulator. By fitting the model to the experimental data, it is possible to extract the motional impedance parameters, R_m, C_m, and L_m.

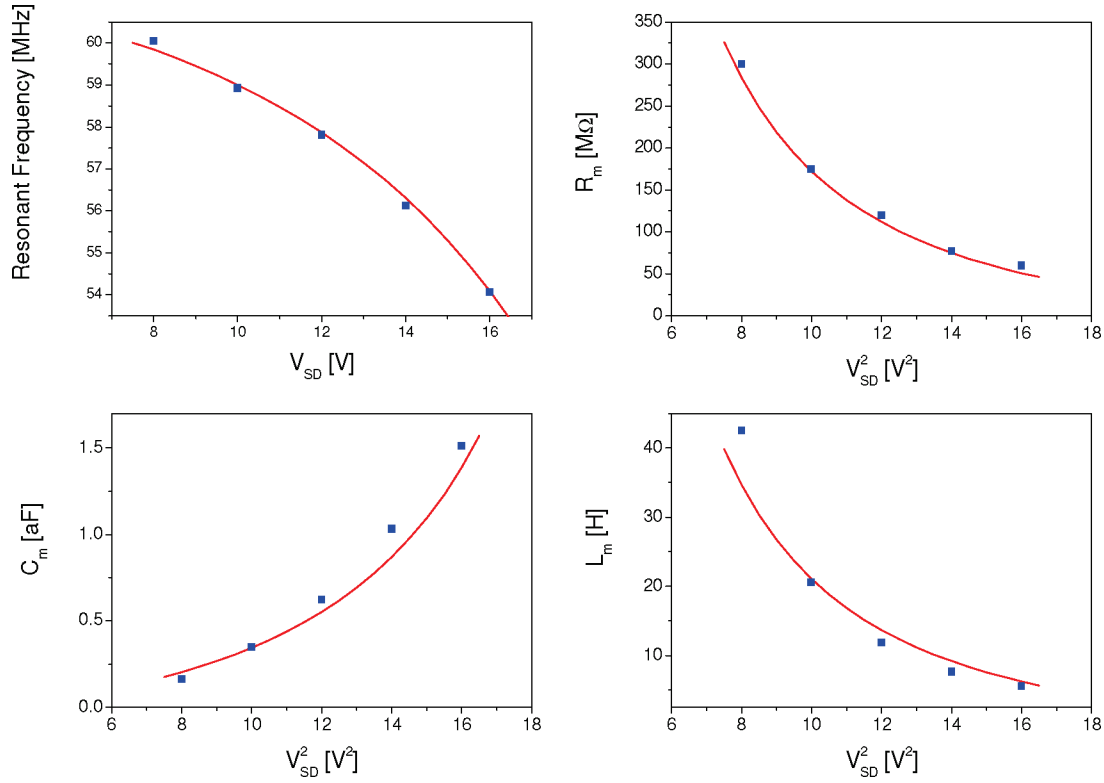

Figure 4. Comparison of the small signal nanotube resonator model to the experimental results. The device geometry was estimated from SEM images. Squares (blue) are measurements, and the red lines are theoretical predictions obtained with CNF Young's modulus $E = 0.41$ TPa, $C_{D0} = 4.5$ aF, and $Q_0 = 47$.

and measured parasitic through-capacitances for our substrate were found to be 350 and 230 aF, respectively. Even with an optimized substrate design, the output levels expected from the small signal model were below parasitic contributions. An operational amplifier circuit was connected to the output of the NEMS resonator to provide a gain of 50 dB. The details of the final circuit design and measurement setup are supplied in the Supporting Information.

The resonance signal from a nanofiber relay is shown in Figure 2 as a function of the source−drain voltage, V_{SD}. The tunability of the resonance peak can be clearly seen. The frequency shift shows the expected V_{SD}^2 dependence up to relatively high bias voltages (>15 V), Figure 2c. Beyond this, the measured frequency appears to saturate and, in some cases, even increases (see data points at 18 V in Figure 2b). There are two possible reasons for such behavior. The first is the "guitar" effect,[15] where the electrostatic force induces tension in the CNF that increases the resonance frequency. The second possibility is that the CNF has come into contact with impurity particles present at the source electrode, thereby effectively shortening its suspended length and increasing the resonant frequency. Although we can be sure that we have a large nanofiber resonator in place before the measurements, we cannot completely rule out the presence of much smaller structures at the source electrode that can also be deposited during the nanofiber deposition step. SEM images of the devices after operation indicate the presence of such structures. The data in Figure 2c indicate the

likelihood of the second explanation because the reverse scan frequencies are simply shifted slightly upward in frequency but show the same slope as for the forward scan.

Experimentally, the motional impedance parameters are extracted from the measurements by simulating the entire system in the ADS circuit simulator, where the operational amplifier circuit was represented by a SPICE model and the series resonator was embedded in circuit parameters measured for the coplanar layout on the MgO substrate. The fit to the small signal model is very good, confirming that the device can be modeled as a series resonator. Examples of the fit to the transmission signal and the phase are shown in Figure 3 for the higher frequency device at a source−drain voltage of 17 V, yielding $R_m = 82$ MΩ, $C_m = 1.45$ aF, and $L_m = 5.7$ H.

The loaded Q-factors that were extracted from the fitted motional impedance parameters are quite low, ranging from $Q_L = 54$ for $V_{SD} = 8$ V to $Q_L = 22$ at $V_{SD} = 18$ V, Figure 2d. The highest Q-factors we have measured are on the order of 200. However, a more reproducible and better controlled fabrication procedure, yielding cleaner devices, will be necessary to significantly improve the operation. The qualitative trend in Q_L is also as expected, Figure 2d, but again there appears to be evidence of a change in device behavior as the source−drain voltage is increased on the first scan.

The results of a quantitative comparison between the theoretical and experimental small signal model parameters are illustrated in Figure 4. Here we have chosen to compare the experimental data up to $V_{SD} = 16$ V, covering the upward voltage sweep range where the resonance frequency shifts with V_{SD}^2, as expected. The dimensions of the resonator were estimated from SEM pictures, taken after the device was coated with a thin gold film to avoid charging, CNF length = 2.05 μm, CNF diameter = 100 nm, giving an effective mass of 3.4 fg, and initial height above drain electrode = 120 nm. The theoretical model has three adjustable parameters: the Young's modulus of the CNF, C_{D0}, and Q_0. The comparison is shown for a Young's modulus of 0.41 TPa, $C_{D0} = 4.5$ aF, and $Q_0 = 47$. The fitted Young's modulus is within the expected range for CNF. The quantitative agreement is very good for the resonant frequency and R_m dependence. The agreement between the measured and calculated C_m and L_m shows slightly more scatter but is still quite good.

We have demonstrated the first direct transmission measurements on individual, singly clamped CNF resonators using a broadband capacitive coupling technique and shown the tuning of the resonant frequency with the applied source−drain dc voltage. The results are in good agreement with a small signal model and provide valuable input for evaluating the usefulness of carbon nanotube and nanofiber NEMS for applications in electronics. The method should be applicable to smaller MWNT devices with appropriate changes to the amplifier circuit to move the broadband detection window to higher frequencies. The difficulty resides with observing the device before measurement, essential if a deposition fabrication technique is used. The problem could be overcome if the nanotube device could be reliably grown in the desired position with the desired geometry. Work toward this goal is in progress.

Acknowledgment. We are grateful for helpful discussions with A. Deleniv, P. Delsing, D. Dubuc, F. Kusidlo, P. Linnér, A. Masud, B. Starmark, M. Sveningsson, Y. Tarakanov, J. Wallinheimo, and B. Witkamp. Financial support from the EU NANORF STREP programme, The Knut and Alice Wallenberg Foundation, the Swedish Strategic Research Foundation, the Korea Research Foundation Grant funded by the Korean Government (MOEHD), and Nokia Research Center is gratefully acknowledged. This paper reflects the views of the authors and not necessarily those of the EC. The community is not liable for any use that may be made of the information contained herein.

Supporting Information Available: Measurement Circuit. This material is available free of charge via the Internet at http://pubs.acs.org.

References

(1) Cleland, A. N. *Foundations of Nanomechanics*; Springer-Verlag: Berlin, 2003.
(2) http://www.itrs.net/reports.html, 2007 edition (accessed January 2008).
(3) Jonsson, L. M.; Axelsson, S.; Nord, T.; Viefers, S.; Kinaret, J. M. *Nanotechnology* **2004**, *15*, 1497–1502.
(4) Lee, S. W.; Lee, D. S.; Morjan, R. E.; Jhang, S. H.; Sveningsson, M.; Nerushev, O. A.; Park, Y. W.; Campbell, E. E. B. *Nano Lett.* **2004**, *4*, 2027–2030.
(5) Dujardin, E.; Derycke, V.; Goffman, M. F.; Lefèvre; Bourgoin, J. P. *Appl. Phys. Lett.* **2005**, *87*, 193107.
(6) Jang, J. E.; Cha, S. N.; Choi, Y. J.; Kang, D. J.; Butler, T. P.; Hasko, D. G.; Jung, J. E.; Kim, J. M.; Amaratunga, G. A. J. *Nat. Nanotechnol.* **2008**, *3*, 26–30.
(7) Kim, P.; Lieber, C. M. *Science* **1999**, *286*, 2148.
(8) Kaul, A. B.; Wong, E. W.; Epp, L.; Hunt, B. D. *Nano Lett.* **2006**, *6*, 942–947.
(9) Rueckes, T.; Kim, K.; Joselevich, E.; Tseng, G. Y.; Cheung, C.-L.; Lieber, C. M. *Science* **2000**, *289*, 94–97.
(10) Fennimore, A. M.; Yuzvinsky, T. D.; Han, W. O.; Fuhrer, M. S.; Cumings, J.; Zettl, A. *Nature* **2003**, *424*, 408–410.
(11) Cohen-Karni, T.; Segev, L.; Srur-Lavi, O.; Cohen, S. R.; Joselevich, E. *Nat. Nanotechnol.* **2006**, *1*, 36–41.
(12) Sazanova, V.; Yaish, Y.; Ustinel, H.; Roundy, D.; Arias, T. A.; McEuen, P. L. *Nature* **2003**, *431*, 284–287.
(13) Witkamp, B.; Poot, M.; van der Zant, H. S. J. *Nano Lett.* **2006**, *6*, 2904–2908.
(14) Peng, H. B.; Chang, C. W.; Aloni, S.; Yuzvinsky, T. D.; Zettl, A. *Phys. Rev. Lett.* **2006**, *97*, 087203.
(15) Purcell, S. T.; Vincent, P.; Journet, C.; Binh, V. T. *Phys. Rev. Lett.* **2002**, *89*, 276103.
(16) Jensen, K.; Weldon, J.; Garcia, H.; Zettl, A. *Nano Lett.* **2007**, *7*, 3508–3511.
(17) Truitt, P. A.; Hertzberg, J. B.; Huang, C. C.; Ekinci, K. L.; Schwab, K. C. *Nano Lett.* **2007**, *7*, 120–126.
(18) Isacsson, A.; Kinaret, J. M.; Kaunisto, R. *Nanotechnology* **2007**, *18*, 195203.
(19) Lee, S. W.; Lee, D. S.; Yu, H. Y.; Campbell, E. E. B.; Park, Y. W. *Appl. Phys. A: Mater. Sci. Process.* **2004**, *78*, 283–286.
(20) Morjan, R. E.; Kabir, M. S.; Lee, S. W.; Nerushev, O. A.; Lundgren, P.; Bengtsson, S.; Park, Y. W.; Campbell, E. E. B. *Curr. Appl. Phys.* **2004**, *4*, 591–594.
(21) Husain, A.; Hone, J.; Postma, H. W. C.; Huang, X. M. H.; Drake, T.; Barbic, M.; Scherer, A.; Roukes, M. L. *Appl. Phys. Lett.* **2003**, *83*, 1240–1242.

NL080345W